

Peltier cooling in molecular junctions

Longji Cui¹, Ruijiao Miao¹, Kun Wang¹, Dakotah Thompson¹, Linda Angela Zotti²,
Juan Carlos Cuevas^{2,3*}, Edgar Meyhofer^{1*} and Pramod Reddy^{1,4*}

The study of thermoelectricity in molecular junctions is of fundamental interest for the development of various technologies including cooling (refrigeration) and heat-to-electricity conversion^{1–4}. Recent experimental progress in probing the thermopower (Seebeck effect) of molecular junctions^{5–9} has enabled studies of the relationship between thermoelectricity and molecular structure^{10,11}. However, observations of Peltier cooling in molecular junctions—a critical step for establishing molecular-based refrigeration—have remained inaccessible. Here, we report direct experimental observations of Peltier cooling in molecular junctions. By integrating conducting-probe atomic force microscopy^{12,13} with custom-fabricated picowatt-resolution calorimetric microdevices, we created an experimental platform that enables the unified characterization of electrical, thermoelectric and energy dissipation characteristics of molecular junctions. Using this platform, we studied gold junctions with prototypical molecules (Au–biphenyl–4,4′–dithiol–Au, Au–terphenyl–4,4′–dithiol–Au and Au–4,4′–bipyridine–Au) and revealed the relationship between heating or cooling and charge transmission characteristics. Our experimental conclusions are supported by self-energy-corrected density functional theory calculations. We expect these advances to stimulate studies of both thermal and thermoelectric transport in molecular junctions where the possibility of extraordinarily efficient energy conversion has been theoretically predicted^{2–4,14}.

When an electrical current flows across an isothermal junction of two materials, net refrigeration is accomplished when Peltier cooling is larger in magnitude than Joule heating^{15,16}. Experimentally probing Peltier cooling and Joule heating in current-carrying molecular junctions is crucial for understanding electron transport, electron–phonon interactions and energy dissipation mechanisms at the atomic and molecular scales. Previous experimental studies^{17–19} have explored local ionic and electronic heating in molecular junctions and probed the non-equilibrium temperature increase due to electron–phonon and electron–electron interactions in the junctions. More recently, experimental advancements have enabled the measurement of Joule heating in the electrodes of molecular junctions^{20,21}. In spite of interesting theoretical predictions and the practical significance^{14,22}, experimental observations of molecular-scale refrigeration have not been possible because of technical challenges in detecting picowatt-level cooling.

We developed an experimental platform that is suitable for creating and stably maintaining molecular junctions while allowing simultaneous measurements of the electrical conductance and Seebeck coefficient, as well as the heating or cooling power deposited in the electrodes of the molecular junctions. Specifically, we developed custom-fabricated calorimetric microdevices (Fig. 1a,b), which have

integrated into them highly sensitive platinum thermometers with a temperature resolution (ΔT_{\min}) of <0.1 mK (see Supplementary Fig. 1 and Supplementary Section 11). The microdevice is suspended by four long, doubly clamped silicon nitride beams to achieve both high thermal resistance ($R_s \approx 3.3 \times 10^6$ K W⁻¹; Supplementary Fig. 2) and stiffness (~ 3.8 N m⁻¹; Supplementary Fig. 5). These characteristics enable detection of heating or cooling power with ~ 30 pW resolution. Moreover, the planar surface of the microdevice (Supplementary Fig. 3) is coated with an electrically isolated Au layer, on top of which a self-assembled monolayer is created to aid the formation of molecular junctions (see Fig. 1a and Methods).

Our strategy for quantifying the Peltier-effect-based cooling of molecular junctions, at room temperature (298 K), is depicted in Fig. 1a. A contact-mode atomic force microscope (AFM), equipped with a sharp Au-coated cantilevered probe (tip radius ~ 100 nm and stiffness ~ 0.1 N m⁻¹; see Supplementary Fig. 4), is used to make a ‘soft’ contact with the monolayer of molecules on the Au-coated microdevice such that the contact force is maintained at ~ 1 nN by using feedback control. As established in past work^{12,13,23,24}, this nanoscopic contact between an AFM tip and a self-assembled monolayer contains approximately 100 metal–molecule–metal junctions (see Supplementary Section 8). Next, we applied a voltage bias (V_p) and recorded the resultant electric current (I) flowing through the molecules from which we obtained the electrical conductance (and the I – V characteristics) of the molecular junctions. Current flow across the molecular junctions results in heat dissipation and cooling due to Joule heating and Peltier effects, which in turn give rise to a temperature change (ΔT) of the calorimetric microdevice that can be quantified by measuring the resistance of the Pt thermometer integrated into the device. To monitor the temperature change, we supplied a fixed electric current ($I_{\text{in}} = 20$ μ A) to the Pt thermometer while continuously monitoring the voltage drop (V_{cal}) across the resistor. The total cooling or heating power (Q_{cal}) in the calorimeter can be directly determined from ΔT by $Q_{\text{cal}} = \Delta T/R_s$, where $R_s \approx 3.3 \times 10^6$ K W⁻¹ is the thermal resistance of the microdevice (see Supplementary Fig. 2).

One may ask whether it is reasonable to expect cooling in the electrodes of molecular junctions and under which conditions. Within Landauer theory, when a voltage bias V_p is applied to the probe relative to the grounded calorimeter electrode, the power input into the calorimeter (Q_{cal}) is²⁴

$$Q_{\text{cal}}(V_p) = \frac{2}{h} \int_{-\infty}^{\infty} (\mu_{\text{cal}} - E) \tau(E, V_p) [f_{\text{cal}} - f_p] dE \quad (1)$$

$$= GTSV_p + \frac{1}{2}GV_p^2 + O(V_p^3)$$

¹Department of Mechanical Engineering, University of Michigan, Ann Arbor, MI, USA. ²Departamento de Física Teórica de la Materia Condensada and Condensed Matter Physics Center (IFIMAC), Universidad Autónoma de Madrid, Madrid, Spain. ³Department of Physics, University of Konstanz, Konstanz, Germany. ⁴Department of Materials Science and Engineering, University of Michigan, Ann Arbor, MI, USA. *e-mail: juancarlos.cuevas@uam.es; meyhofer@umich.edu; pramodr@umich.edu

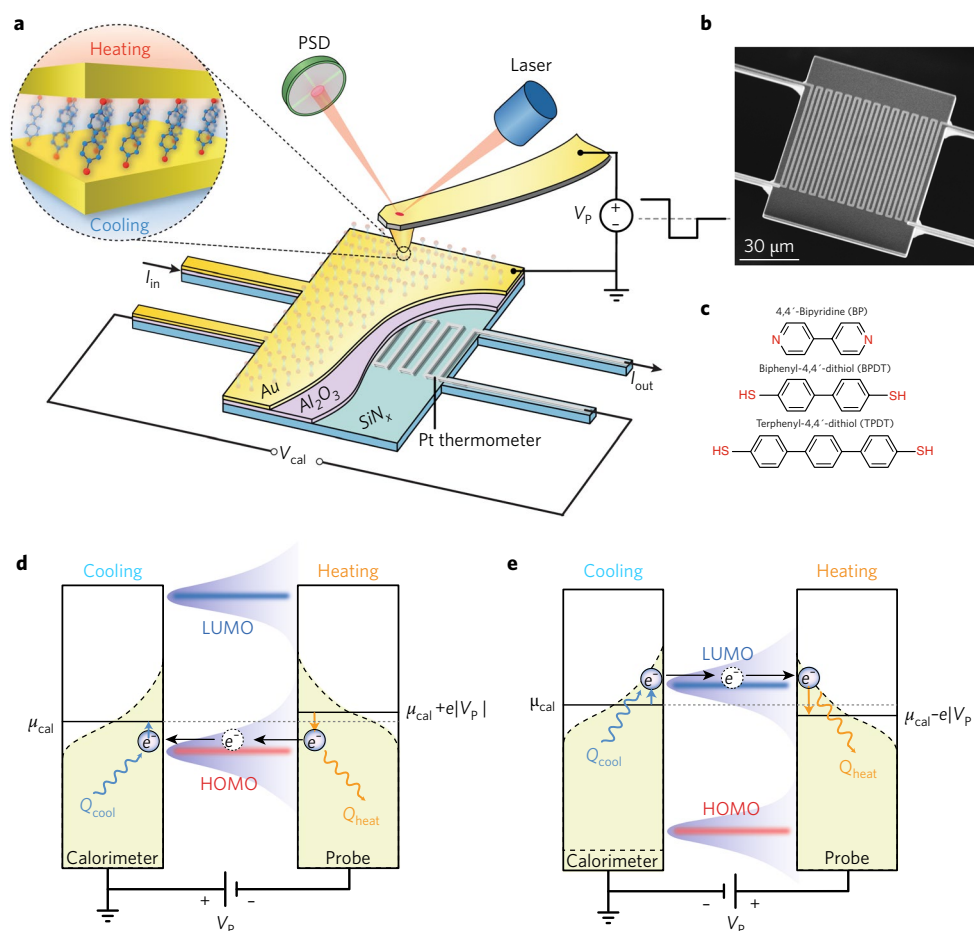


Fig. 1 | Probing cooling in molecular junctions. **a**, Schematic of the experimental platform. Molecular junctions are formed by placing a Au-coated AFM tip in gentle contact with a self-assembled monolayer created on a Au-coated calorimetric microdevice. The electrical conductance of the molecular junctions is measured by supplying a small voltage bias (V_p) and recording the resultant current. The temperature change of the microdevice is induced by the heating or cooling effect in the current-carrying molecular junctions. The resistance of the Pt thermometer is continuously monitored by applying an electric current (I_{in}) into the resistor and measuring the voltage output (V_{cal}). PSD, position-sensitive detector. **b**, Scanning electron microscope image of the custom-fabricated microdevice. **c**, Chemical structures of the molecules studied in this experiment. **d**, Schematic description of the origin of the Peltier effect in a molecular junction in which transport is dominated by the HOMO. The transmission function is depicted as a Lorentzian around the HOMO and LUMO levels. The terms μ_{cal} , Q_{heat} and Q_{cool} denote chemical potential, heating and cooling power, respectively. **e**, Same as **d**, but for the LUMO-dominated case.

where μ_{cal} is the chemical potential of the calorimeter electrode, f_p and f_{cal} are the Fermi–Dirac distributions of the probe and calorimeter electrodes, respectively, $\tau(E, V_p)$ is the energy- (E) and voltage-bias-dependent transmission of the junction, T is absolute temperature, G and S are the low-bias electrical conductance and the Seebeck coefficient of the molecular junctions, respectively, and $O(V_p^3)$ represents the higher-order terms. Note that G and S are related to $\tau(E, V_p)$ (see Methods). Thus, for small biases, when $|V_p| < 2|ST|$ and the first-order term $GTSV_p$ dominates, cooling is expected when SV_p , the product of the Seebeck coefficient and the applied bias, is negative. The physical picture behind the expected cooling mechanism is shown in the schematics in Fig. 1d,e and is discussed below.

We first investigated cooling in Au–biphenyl-4,4'-dithiol (BPDT)–Au junctions. Towards this goal, we applied a periodic, three-level voltage sequence, $+V_p$ (from $t=0$ to 1.66 s), $-V_p$ (1.66 s to 3.33 s) and 0 volts (3.33 s to 5 s), across Au–BPDT–Au junctions, and simultaneously measured both the current flow through the junctions and Q_{cal} (note that the calorimeter electrode is always grounded in these experiments). The time period of each of the voltage pulses (1.66 s) is chosen to be significantly larger than the thermal time constant (~ 40 ms) of the microdevice

(Supplementary Fig. 2) so that there is sufficient time for steady-state conditions to be established in the calorimeter. Representative traces of the recorded electrical current (I) and heating or cooling power (Q_{cal}), corresponding to one period of the three-level voltage sequence ($+V_p$, $-V_p$ and 0, where V_p was chosen to be 3 mV), are shown in Fig. 2a. It can be clearly seen that when the voltage is changed from $+V_p$ to $-V_p$, the current direction switches sign as expected. However, the expected heating or cooling of the calorimeter (represented by a temperature change of the calorimeter) remains unresolvable owing to the considerable noise in the signal. To resolve the desired signal, we used an averaging scheme that improves the thermal resolution and hence the calorimetric resolution (see Supplementary Section 11 for details). Briefly, in this approach the thermal signals from many (500 to 2,000) equivalent phases of three-level voltage sequence ($+V_p$, $-V_p$ and 0) are aligned and averaged, and Q_{cal} is determined. Figure 2a depicts the results obtained after averaging 10, 100 and 1,500 period traces, clearly demonstrating that such averaging reduces noise to a level where heating and cooling can be resolved. Specifically, for Au–BPDT–Au junctions we find a net cooling power ~ 300 pW when a negative bias of -3 mV is applied. The corresponding heating power when reversing the bias polarity is ~ 600 pW.

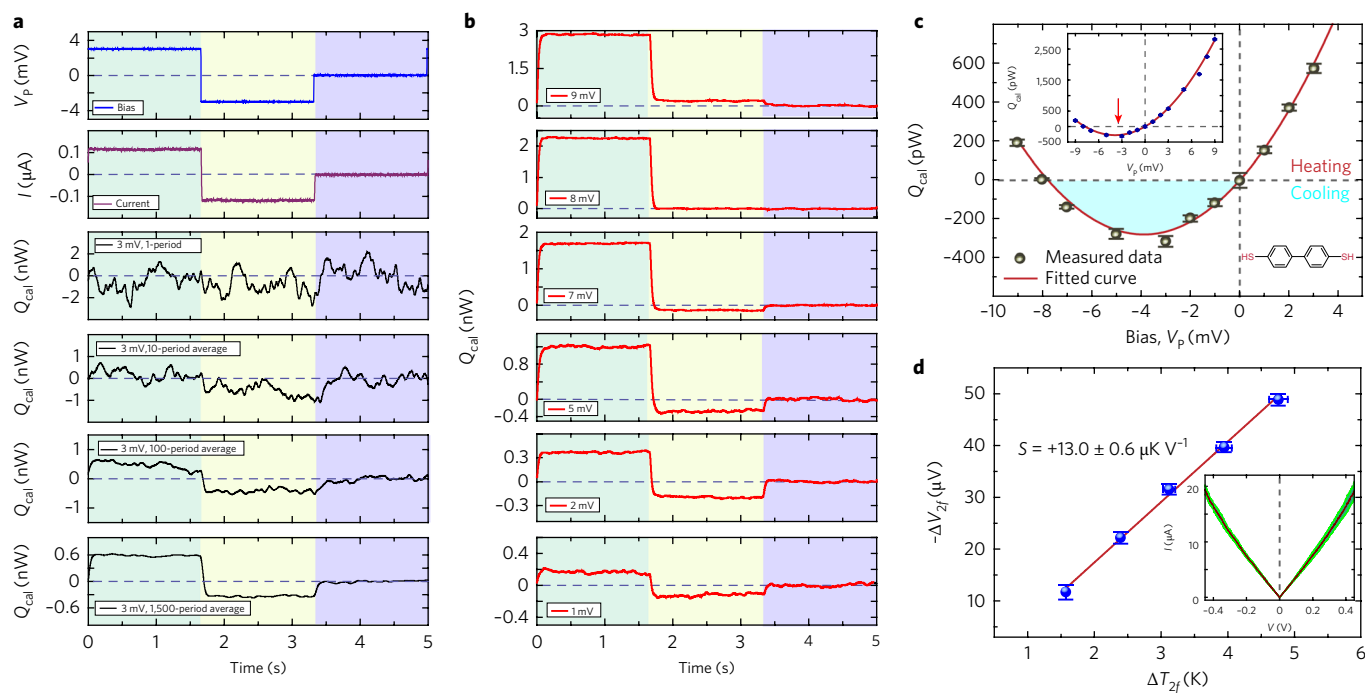


Fig. 2 | Observation of Peltier cooling in Au-BPDT-Au junctions. **a**, Experimental protocol for quantifying the heating and cooling power in molecular junctions. A periodic three-level voltage (blue line) is supplied into the junctions, while electrical current (purple line) and thermal signal (black lines) are simultaneously recorded. Improved thermal resolution is obtained by averaging the thermal signal over a large number of periods to reduce noise level. **b**, Time-averaged heating and cooling signal traces (red lines) under different voltage bias. **c**, Measured voltage-dependent thermal power for BPDT junctions. The solid red line indicates the fitted curve using equation (1) and the measured Seebeck coefficient and electrical conductance. The shaded blue region indicates the voltage region where net cooling (refrigeration) is observed. Inset shows the measured data and the fitted curve for voltage bias from -9 mV to $+9$ mV. The red arrow points to the voltage that leads to the maximum cooling effect. Error bars represent the standard deviation of data obtained from the time-averaging scheme. **d**, Measured Seebeck coefficient (S) of BPDT junctions. The red solid line is the best linear fit to the measured data, with the slope indicating the Seebeck coefficient. Inset shows the I - V characteristics of the junctions obtained by averaging ten individual I - V curves. The green shaded region represents the standard deviation. Error bars represent the standard deviation of data obtained from five independent measurements.

Figure 2b presents the time-averaged thermal signal for varying V_p from 1 mV and 9 mV for the same Au-BPDT-Au molecular junctions. It can be seen that, under positive biases, Q_{cal} is always positive. In contrast, net cooling ($Q_{\text{cal}} < 0$) is observed in a narrow range of negative biases, $V_p \in [-8$ mV, 0 mV]. We plot the measured Q_{cal} as a function of the voltage bias applied to the probe (V_p) in Fig. 2c. The measured power dissipation is roughly parabolic as expected from equation (1). To obtain a quantitative comparison with the predictions of equation (1), we independently measured the electrical conductance and the Seebeck coefficient of molecular junctions. These measurements are accomplished with the same experimental platform (see Methods) by directly recording the I - V characteristics and S . From these measurements (Fig. 2d), we determined that the low-bias conductance is $\sim 37 \mu\text{S}$ (note that this relatively large conductance is due to the fact that we trapped multiple molecules in the molecular junction) and the Seebeck coefficient is $+13.0 \pm 0.6 \mu\text{V K}^{-1}$ (indicating that transport is dominated by the highest occupied molecular orbital, HOMO), in good agreement with past work¹² for Au-BPDT-Au molecular junctions. By putting these independently measured transport parameters into equation (1) (neglecting higher-order $O(V_p^3)$ terms), we obtained the solid line shown in Fig. 2c. The resulting agreement between the calculated thermoelectric cooling of Au-BPDT-Au junctions and the experimental values confirms the applicability of the Landauer approach for modelling cooling.

The physical processes that result in molecular-junction-based cooling can be understood by considering the schematic of a HOMO junction shown in Fig. 1d. The left electrode is grounded and represents the electrode integrated into the calorimeter while

the right electrode signifies the probe. When the probe is negatively biased as shown, electrons are injected into the probe electrode at an energy of $\mu_{\text{cal}} + e|V_p|$ and leave the calorimeter electrode at an energy μ_{cal} . Under these conditions, charge transfer occurs not only at energies between $\mu_{\text{cal}} + e|V_p|$ and μ_{cal} but also at energies within a few $k_B T$ (k_B is the Boltzmann constant) of the chemical potentials owing to the thermal broadening of the Fermi-Dirac functions. Charge transfer at energies between the chemical potentials leads to Joule heating in the calorimeter (see Supplementary Fig. 10). However, charge transfer through the junction at energies below the chemical potential of the calorimeter electrode leads to cooling in the calorimeter, while charge transfer at energies above the chemical potential of the probe leads to heating. Thus, in HOMO-dominated junctions, when the probe is negatively biased and the voltage magnitude is appropriately chosen, net cooling (that is, Peltier cooling dominates over Joule heating) occurs in the calorimeter, as the transmission probabilities (see Fig. 1d) are larger at μ_{cal} than at $\mu_{\text{cal}} + e|V_p|$ (see Supplementary Section 12 for more details of the physical mechanism). The situation is reversed when the probe is positively biased, resulting in only net heating in the calorimeter for HOMO-dominated junctions. Similar arguments can be presented to understand cooling in LUMO-dominated junctions (Fig. 1e).

Corresponding measurements were also performed on Au-terphenyl-4,4'-dithiol (TPDT)-Au junctions and Au-Au nanocontacts. The measured thermal power, I - V characteristics and Seebeck coefficient are summarized in Fig. 3. In contrast to the BPDT case, TPDT molecular junctions exhibit significantly smaller cooling owing to their low electrical conductance, in spite of a slightly higher Seebeck coefficient of $+15.7 \pm 1.1 \mu\text{V K}^{-1}$. In Au-Au nanocontacts

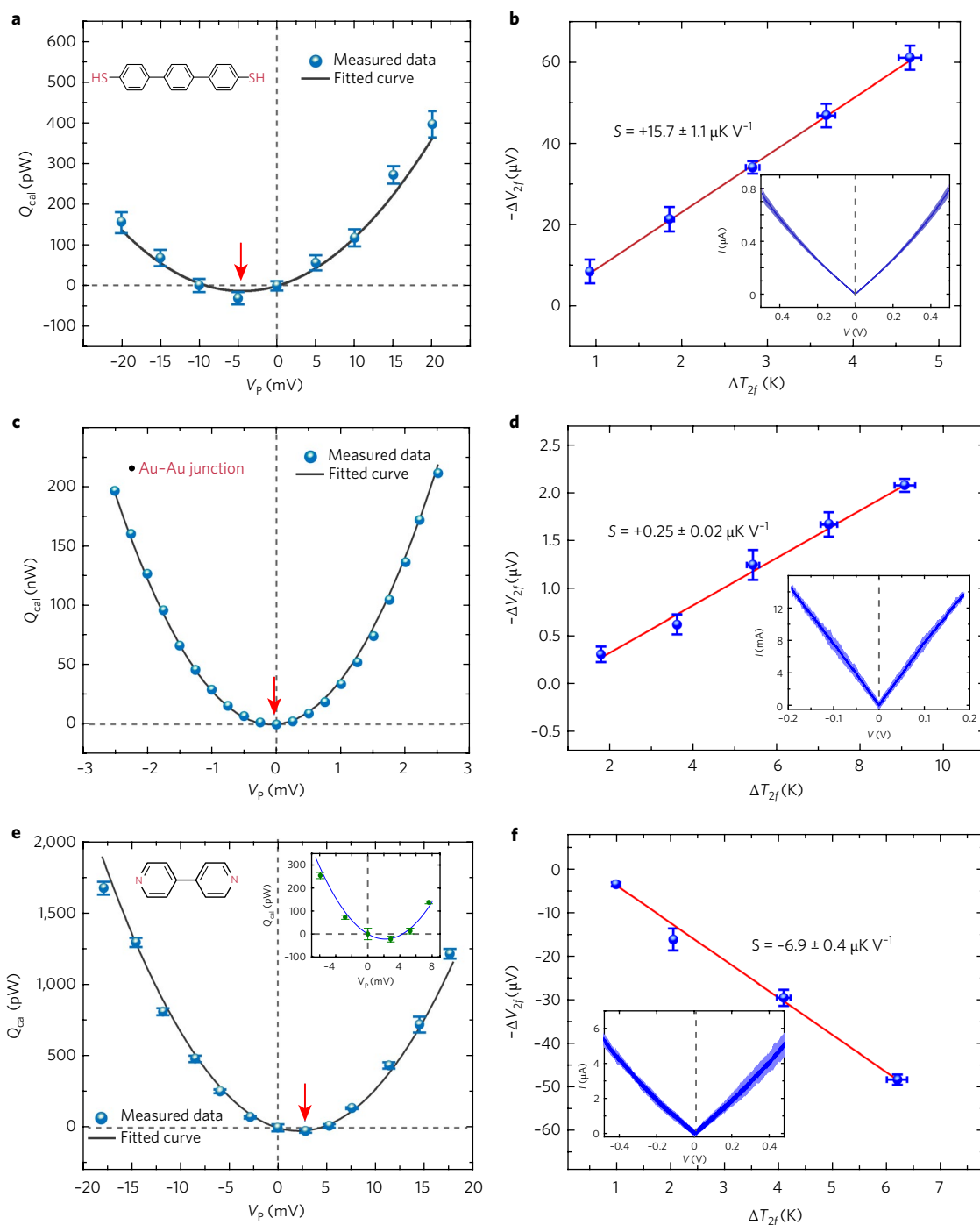


Fig. 3 | Measured Peltier effect in Au-TPDT-Au, Au-Au and Au-BP-Au junctions. a, b, As in Fig. 2c and d, but for TPDT junction. The black solid line indicates the fitted curve using transport parameters (low-bias conductance and Seebeck coefficient) input from independent characterizations of both properties. **c, d,** For Au-Au noncontacts in which negligible cooling effect is found. **e, f,** For BP junction. In contrast to BPDT and TPDT junctions, the maximum in cooling power is observed when a positive bias is applied, consistent with the physical picture of the Peltier effect in LUMO-dominated molecular junctions (indicated by negative Seebeck coefficient in **f**). Error bars in **a, c, e** represent the standard deviation of data obtained from the time-averaging scheme. Error bars in **b, d, f** represent the standard deviation of data obtained from five independent measurements.

without molecules between the Au electrodes, there was no detectable cooling effect (Fig. 3c) because of the extremely small Seebeck coefficient—a result in excellent agreement with the prediction of equation (1). This control experiment confirms that the molecules play a critical role in the observed cooling.

Finally, we performed measurements using Au-4,4'-bipyridine (BP)-Au molecular junctions, in which transport is expected to be

dominated by the LUMO level⁹ (as also confirmed by our measurements of the Seebeck coefficients; see Fig. 3f). In these experiments, in contrast to the measurements in HOMO-dominated junctions, we observed net cooling in the calorimeter for a positive bias applied to the probe (Fig. 3e). The observed heat dissipation characteristics of Au-BP-Au junctions are consistent with the predictions of equation (1) using independent measurements of the electrical

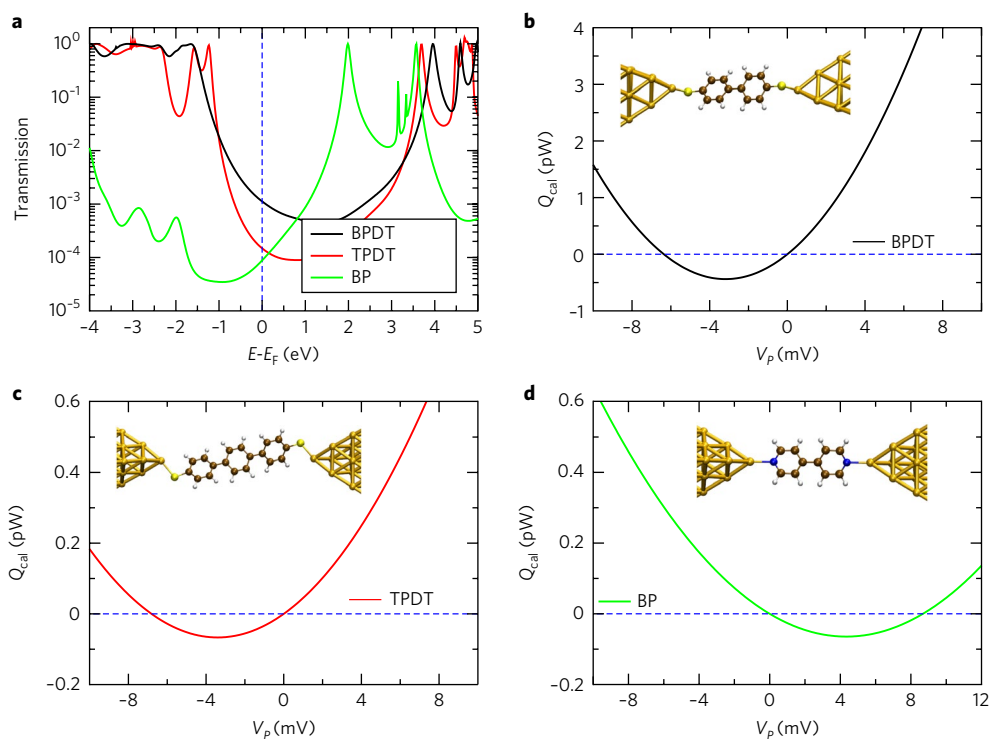


Fig. 4 | Computed heating/cooling effect in the molecular junctions used in this experiment. **a**, Calculated zero-bias transmission function as a function of energy, measured with respect to the Fermi energy (E_F), for BPDT, TPDT and BP junctions. The transmission and its derivative at E_F determine the electrical conductance and the Seebeck coefficient of the molecular junctions, respectively. **b–d**, Calculated heating and cooling power at different voltages for BPDT, TPDT and BP single-molecule junctions, respectively. The insets show the geometries used to compute the different transport properties.

conductance and the Seebeck coefficient, as reflected by the excellent agreement between the experimental data and the result from equation (1). The physical picture for the observed cooling behaviour in LUMO-dominated junctions is shown in Fig. 1e.

To identify the microscopic origin of the observed heating and cooling effects in our molecular junctions, we used an ab initio transport model based on density functional theory²⁵ (DFT) to compute the transmission function ($\tau(E)$). To investigate whether our experimental observations are directly determined by the structure and properties of the molecules incorporated into the junction, we focus our computational analysis on single-molecule junctions. In Fig. 4a, we summarize the results for the zero-bias transmission function for three junctions where the molecules under study (BPDT, TPDT and BP) are attached to Au electrodes via atop positions (insets in Fig. 4b–d). For these calculations, we used the DFT + Σ method to attenuate known self-interaction errors in DFT and account for image charge effects^{21,26} (see Methods). Then, using $\tau(E)$, we computed within the Landauer theory (see Methods) the electrical conductance, the Seebeck coefficient and the power released in the calorimeter (equation (1)). As we are interested in the low-bias regime, the bias-dependence of the transmission was ignored.

For the Au–BPDT–Au and Au–TPDT–Au junctions, the transport at the Fermi energy (E_F) is dominated by the HOMO of the molecules (Fig. 4a), which results in a negative slope of the transmission at E_F and a positive Seebeck coefficient. In this example, the conductance of the BPDT junction is $1.1 \times 10^{-3} G_0$, where $G_0 = 2e^2/h = 12.9 \text{ k}\Omega^{-1}$ is the conductance quantum, while for TPDT the conductance is $1.5 \times 10^{-4} G_0$, almost an order of magnitude lower as expected from the exponential decay of the conductance with molecular length. The corresponding Seebeck coefficients at room temperature are $+10.5 \mu\text{V K}^{-1}$ for BPDT

and $+11.1 \mu\text{V K}^{-1}$ for TPDT, which are in good accord with our experimental observations. The results for the computed cooling power in single-molecule junctions (Fig. 4b and c) predict that these junctions exhibit cooling for negative bias in a voltage range of $V_p \in [-7 \text{ mV}, 0 \text{ mV}]$, in excellent agreement with the voltage range for which cooling is observed in the experiments. The lower cooling power of TPDT is simply due to its lower conductance. Note that the difference in power values with respect to the experiments arises because we are simulating single-molecule junctions instead of the many-molecule junctions used in the work. Finally, the BP junction exhibits a conductance of $8.8 \times 10^{-5} G_0$, consistent with previous experimental and theoretical work⁹, transport is dominated by the LUMO (Fig. 4a), with a negative Seebeck coefficient of $-14.4 \mu\text{V K}^{-1}$, and the cooling effect occurs at positive bias (Fig. 4d) in a range $V_p \in [0 \text{ mV}, +9 \text{ mV}]$, again in qualitative agreement with our observations. A direct quantitative comparison between theory and experiments is primarily limited by the uncertainty in the number of molecules in the junction (note, however, that the Seebeck coefficient is independent of the number of molecules). These results strongly indicate that the observed cooling and heating are determined by the intrinsic properties of individual molecules.

In conclusion, we have experimentally observed cooling in molecular junctions. Our experimental results also link the charge transmission characteristics of a molecule to the Peltier effects measured in molecular junctions. Furthermore, the experimental platform reported here allows the seamless characterization of electrical, thermal and thermoelectric transport properties on the same molecular junction in a unified manner. This work should stimulate further systematic exploration of atomic- and molecular-scale thermal transport^{11,27–29} and quantification of the thermoelectric figure of merit^{2–4,14} in a variety of interesting molecules, nanostructures and materials.

Methods

Methods, including statements of data availability and any associated accession codes and references, are available at <https://doi.org/10.1038/s41565-017-0020-z>.

Received: 12 August 2017; Accepted: 24 October 2017;

Published online: 18 December 2017

References

1. Dubi, Y. & Di Ventra, M. Colloquium: Heat flow and thermoelectricity in atomic and molecular junctions. *Rev. Mod. Phys.* **83**, 131–155 (2011).
2. Finch, C. M., García-Suárez, V. M. & Lambert, C. J. Giant thermopower and figure of merit in single-molecule devices. *Phys. Rev. B* **79**, 033405 (2009).
3. Bergfield, J. P., Solis, M. A. & Stafford, C. A. Giant thermoelectric effect from transmission supernodes. *ACS Nano* **4**, 5314–5320 (2010).
4. Karlström, O., Linke, H., Karlström, G. & Wacker, A. Increasing thermoelectric performance using coherent transport. *Phys. Rev. B* **84**, 113415 (2011).
5. Kim, Y., Jeong, W., Kim, K., Lee, W. & Reddy, P. Electrostatic control of thermoelectricity in molecular junctions. *Nat. Nanotech.* **9**, 881–885 (2014).
6. Li, Y., Xiang, L., Palma, J., Asai, Y. & Tao, N. J. Thermoelectric effect and its dependence on molecular length and sequence in single DNA molecules. *Nat. Commun.* **7**, 11294 (2016).
7. Reddy, P., Jang, S. Y., Segalman, R. A. & Majumdar, A. Thermoelectricity in molecular junctions. *Science* **315**, 1568–1571 (2007).
8. Rincón-García, L. et al. Molecular design and control of fullerene-based bi-thermoelectric materials. *Nat. Mater.* **15**, 289–293 (2016).
9. Widawsky, J. R., Darancet, P., Neaton, J. B. & Venkataraman, L. Simultaneous determination of conductance and thermopower of single molecule junctions. *Nano Lett.* **12**, 354–358 (2012).
10. Aradhya, S. V. & Venkataraman, L. Single-molecule junctions beyond electronic transport. *Nat. Nanotech.* **8**, 399–410 (2013).
11. Cui, L., Miao, R., Jiang, C., Meyhofer, E. & Reddy, P. Perspective: thermal and thermoelectric transport in molecular junctions. *J. Chem. Phys.* **146**, 092201 (2017).
12. Tan, A. et al. Effect of length and contact chemistry on the electronic structure and thermoelectric properties of molecular junctions. *J. Am. Chem. Soc.* **133**, 8838–8841 (2011).
13. Tan, A., Sadat, S. & Reddy, P. Measurement of thermopower and current-voltage characteristics of molecular junctions to identify orbital alignment. *Appl. Phys. Lett.* **96**, 013110 (2010).
14. Sadeghi, H., Sangtarash, S. & Lambert, C. J. Oligoynes molecular junctions for efficient room temperature thermoelectric power generation. *Nano Lett.* **15**, 7467–7472 (2015).
15. Callen, H. B. *Thermodynamics: An Introduction to the Physical Theories of Equilibrium Thermodynamics and Irreversible Thermodynamics* (Wiley, New York, 1960).
16. Rowe, D. M. *Thermoelectrics Handbook: Macro to Nano* (CRC/Taylor & Francis, Boca Raton, 2006).
17. Huang, Z. et al. Local ionic and electron heating in single-molecule junctions. *Nat. Nanotech.* **2**, 698–703 (2007).
18. Ioffe, Z. et al. Detection of heating in current-carrying molecular junctions by Raman scattering. *Nat. Nanotech.* **3**, 727–732 (2008).
19. Ward, D. R., Corley, D. A., Tour, J. M. & Natelson, D. Vibrational and electronic heating in nanoscale junctions. *Nat. Nanotech.* **6**, 33–38 (2011).
20. Lee, W. et al. Heat dissipation in atomic-scale junctions. *Nature* **498**, 209–212 (2013).
21. Zotti, L. A. et al. Heat dissipation and its relation to thermopower in single-molecule junctions. *New J. Phys.* **16**, 015004 (2014).
22. Galperin, M., Saito, K., Balatsky, A. V. & Nitzan, A. Cooling mechanisms in molecular conduction junctions. *Phys. Rev. B* **80**, 115427 (2009).
23. Wold, D. J. & Frisbie, C. D. Fabrication and characterization of metal–molecule–metal junctions by conducting probe atomic force microscopy. *J. Am. Chem. Soc.* **123**, 5549–5556 (2001).
24. Choi, S. H., Kim, B. & Frisbie, C. D. Electrical resistance of long conjugated molecular wires. *Science* **320**, 1482–1486 (2008).
25. Pauly, F. et al. Cluster-based density-functional approach to quantum transport through molecular and atomic contacts. *New J. Phys.* **10**, 125019 (2008).
26. Quek, S. Y. et al. Amine–gold linked single-molecule circuits: experiment and theory. *Nano Lett.* **7**, 3477–3482 (2007).
27. Segal, D. & Agarwalla, B. K. Vibrational heat transport in molecular junctions. *Annu. Rev. Phys. Chem.* **67**, 185–209 (2016).
28. Cui, L. et al. Quantized thermal transport in single-atom junctions. *Science* **355**, 1192–1195 (2017).
29. Klöckner, J. C., Siebler, R., Cuevas, J. C. & Pauly, F. Thermal conductance and thermoelectric figure of merit of C_{60} -based single-molecule junctions: electrons, phonons, and photons. *Phys. Rev. B* **95**, 245404 (2017).

Acknowledgements

P.R. and E.M. acknowledge funding from the Office of Naval Research (N00014-16-1-2672, instrumentation), the Department of Energy (DE-SC0004871, scanning probe microscopy), and the National Science Foundation (CBET 1509691, ECCS 1407967, calorimetry). L.A.Z. and J.C.C. acknowledge funding from the Spanish MINECO (projects MAT2014-58982-JIN and FIS2014-53488-P, and FIS2017-84057-P). J.C.C. also thanks the Deutsche Forschungsgemeinschaft, the research programme SFB767 for sponsoring his stay at the University of Konstanz as Mercator Fellow. We acknowledge the Lurie Nanofabrication Facility and Michigan Center for Materials Characterization for facilitating the fabrication and calibration of devices.

Author contributions

P.R., E.M. and J.C.C. conceived the work. L.C., R.M. and K.W. performed the experiments. D.T. designed and fabricated the devices. L.A.Z. performed the calculations. The manuscript was written by L.C., P.R., E.M. and J.C.C. with comments and inputs from all authors.

Competing interests

The authors declare no competing financial interests.

Additional information

Supplementary information is available for this paper at <https://doi.org/10.1038/s41565-017-0020-z>.

Reprints and permissions information is available at www.nature.com/reprints.

Correspondence and requests for materials should be addressed to J.C.C. or E.M. or P.R.

Publisher's note: Springer Nature remains neutral with regard to jurisdictional claims in published maps and institutional affiliations.

Methods

Preparation and characterization of microdevices. The microdevices were custom-fabricated using standard nanofabrication techniques (Supplementary Fig. 1). The suspended regions ($80\ \mu\text{m} \times 60\ \mu\text{m}$) are connected to the surrounding substrate via thin and long beams that result in a thermal resistance of $\sim 3.3 \times 10^6\ \text{K W}^{-1}$ and a stiffness of $\sim 3.85\ \text{N m}^{-1}$ (see Supplementary Fig. 2 and Supplementary Fig. 6 for details of device characterization and finite element analysis). The planar surface of the microdevice was coated by a thin Au film of $\sim 50\ \text{nm}$ (electron-beam evaporation), on which a self-assembled monolayer of molecules was formed (see Supplementary Fig. 5 for details of surface characterization).

Molecular monolayer preparation and junction formation. To obtain the desired monolayers of molecules, we first prepared dilute ethanol or toluene solutions of BPD, TPDT and BP molecules (purity >95%, Sigma Aldrich). Immediately after the deposition of Au layers on the device surfaces, we immersed the devices in $500\ \mu\text{M}$ solutions to initiate self-assembly of molecules on Au surface. The microdevices were incubated for ~ 12 hours in a nitrogen-filled glove box and, following monolayer formation, they were rinsed thoroughly in ethanol or toluene to remove unbound molecules. Devices were dried in a nitrogen environment. Experiments were performed with commercially available AFM cantilevers from NanoAndMore (ARROW-CONTR, nominal force constant $\sim 0.1\ \text{N m}^{-1}$). Before the experimental measurements, the AFM tips were coated with a thin layer of sputtered Au ($\sim 100\ \text{nm}$) and cleaned by oxygen-plasma to eliminate possible contamination. Measurements were initiated by making a gentle contact with the monolayer of molecules using a contact force of about $1\ \text{nN}$, which prevented penetration of the AFM tip into the monolayer and ensured stable and repeatable molecular junctions with ~ 100 molecules (see Supplementary Section 8 for details of ellipsometry and X-ray photoelectron spectroscopy measurements). This estimate of the number of molecules in the junction (~ 100) was obtained by comparing the measured electrical conductance with previously reported values of the single-molecule electrical conductance. Similar values were also obtained by using a simple, contact-mechanics model based on Hertzian theory^{12,13,23,24}.

Thermoelectric voltage measurement. The Seebeck coefficients of the molecular junctions were measured using an alternating current scheme (Supplementary Fig. 8). Briefly, a sinusoidal electric current at frequency f ($0.5\ \text{Hz}$) was supplied to the Pt resistor, which induced sinusoidal perturbation of the temperature of the suspended microdevice with an amplitude ΔT_{2f} and frequency $2f$. Subsequently, we used a lock-in amplifier (Stanford Research Systems, SR830) to measure the thermoelectric voltage (ΔV_{2f}) at $2f = 1\ \text{Hz}$ arising from the applied ΔT_{2f} . The Seebeck coefficient of the junction (S) was found from $S = S_{\text{Au}} - \Delta V_{2f} / \Delta T_{2f}$, where S_{Au} is the Seebeck coefficient of the Au thin film deposited on our calorimeter, which was assumed to be $\sim 1.76\ \mu\text{V K}^{-1}$ (ref. 30).

Computational techniques. The transmission functions and the different transport properties of the single-molecule junctions used in this work were obtained with our previously published first-principles transport method²⁵. Briefly, this method is based on the combination of DFT and non-equilibrium Green's function (NEGF) techniques, and it is implemented in the quantum-chemistry code TURBOMOLE²¹. The first step in this method is the description of the electronic structure of the junctions within DFT. In our DFT calculations, we used the BP86 exchange-correlation functional²² and the Gaussian basis set def-SVP³³. We made sure that the total energies were converged to a precision better than 10^{-6} atomic units, while in the geometry optimizations we ensured that the maximum norm of the Cartesian gradient reached values below 10^{-4} atomic units. The practical construction of the geometries of the molecular junctions considered in the main text was done as follows. First, the molecules were fully relaxed. Then, they were incorporated in a junction where the electrodes were initially simulated with Au pyramids with 20 atoms each. To be precise, the molecules were bonded in atop positions: that is, they were directly coupled to the apex atoms of the Au electrodes. Subsequently, we did one more geometry optimization by relaxing the

positions of the molecule's atoms and those of the four last atoms in the Au clusters. Next, we increased the size of both Au clusters up to 63 atoms to make sure that the metal–molecule level alignment was correctly described. Finally, the whole central region consisting of the molecule plus the two Au clusters was coupled to semi-infinite Au surfaces, which simulate the metallic leads. These surfaces were described with the same level of DFT (same basis set and same functional) as the Au atoms in the central part of the junction²⁵.

To address the known problems of DFT-based methods in accurately describing the energy gap and metal–molecule level alignment, we used the self-energy-corrected DFT + Σ method that partially cures the self-interaction errors in the standard exchange-correlation functional and, in turn, takes into account image charge effects²⁶. We have described in detail the implementation of this method in past work²¹. Briefly, there are two key steps in this method. First, we shift the HOMO and LUMO of the molecules such that they correspond to the negative ionization potential and to the negative electron affinity, respectively. These two latter energies are computed in separate calculations of the molecule in gas phase. Then, to account for the renormalization of the levels when the molecule is brought into the junction, we shift the energy of the occupied states up in energy and the unoccupied states down in energy. These shifts are calculated by describing the screening of the metallic electrodes in a classical way as the interaction of point charges in the molecule with two perfectly conductive infinite surfaces, as described in detail elsewhere²¹.

The last step in our transport method is the use of the information about the electronic structure of the junctions to determine the zero-bias transmission function. This is done with the help of NEGF techniques, as explained in our past work²¹. Finally, the transmission function was used, in the spirit of the Landauer theory, to compute the different transport properties. In particular, the linear conductance G and Seebeck coefficients S are given by:

$$G = G_0 K_0(T) \quad \text{and} \quad S = -\frac{K_1(T)}{eTK_0(T)} \quad (2)$$

where T is the absolute temperature, e is the electron charge and the coefficients $K_n(T)$ are given by

$$K_n(T) = \int_{-\infty}^{\infty} (E - E_F)^n \tau(E) [-\partial_E f(E, T)] dE.$$

Here, E_F is the Fermi energy, $f(E, T)$ is the Fermi–Dirac function and $\tau(E)$ is the zero-bias transmission function. In our junctions, we have verified that it is sufficient to use the low-temperature expansion of these formulae, which reduce to $G = G_0 \tau(E_F)$ and

$$S = -(\pi^2 k_B^2 T / 3e) [\partial_E \tau(E) / \tau(E)]_{E=E_F},$$

where k_B is the Boltzmann constant and $G_0 = 2e^2/h$ is the electrical conductance quantum. Finally, the power released in the calorimeter was calculated with the help of equation (1) in the text. In particular, we verified that the low-bias expansion of that equation applies in the voltage range investigated in this work.

Data availability. The data that support the findings of this study are available from the corresponding author upon reasonable request.

References

- Lin, S. F. & Leonard, W. F. Thermoelectric power of thin gold films. *J. Appl. Phys.* **42**, 3634–3639 (1971).
- Ahlich, R., Bar, M., Haser, M., Horn, H. & Kolmel, C. Electronic-structure calculations on workstation computers — the program system TURBOMOLE. *Chem. Phys. Lett.* **162**, 165–169 (1989).
- Perdew, J. P. Density-functional approximation for the correlation energy of the inhomogeneous electron gas. *Phys. Rev. B* **33**, 8822–8824 (1986).
- Schafer, A., Horn, H. & Ahlich, R. Fully optimized contracted Gaussian-basis sets for atoms Li to Kr. *J. Chem. Phys.* **97**, 2571–2577 (1992).